Single-Crystal Colloidal Multilayers of Controlled Thickness

P. Jiang, J. F. Bertone, K. S. Hwang, and V. L. Colvin*

Department of Chemistry and Center for Nanoscale Science and Technology, Rice University, MS-60, 6100 Main Street, Houston, Texas 77005

Received February 5, 1999. Revised Manuscript Received April 19, 1999

Materials whose dielectric constant varies spatially with submicrometer periodicity exhibit diffractive optical properties which are potentially valuable in a number of existing and emerging applications. Here, such systems are fabricated by exploiting the spontaneous crystallization of monodisperse silica spheres into close-packed arrays. By reliance on a vertical deposition technique to pack the spherical colloids into close-packed silica−air arrays, high quality samples can be prepared with thicknesses up to 50 μm. These samples are planar and thus suitable for optical characterization. Scanning electron microscopy (SEM) of these materials illustrates the close-packed ordering of the spherical colloids in planes parallel to the substrate; cross-sectional SEM micrographs of the arrays as well as optical methods are used to measure sample thickness and uniformity. Normal-incidence transmission spectra in the visible and near-infrared regions show distinct peaks due to diffraction from the colloidal layers. While these basic optical characteristics are similar to thicker and polycrystalline gravity-sedimented colloidal crystals, the systematic control over the number of colloidal layers allows the effect of sample thickness on the optical spectrum to be studied for the first time.

Introduction

Many novel properties can be engineered in periodic dielectric materials by controlling the symmetry and length scale of a sample's microstructure.[1−6] This idea has been used to engineer microwave optics,[4] and recently these dielectric structures have been termed "photonic band gap" materials. The exciting potential of these structured materials for optical applications has motivated efforts to shrink the length scale of the periodicity to submicrometer sizes.[7−16] Lithographically prepared arrays of alumina rods, for example, were recently used as a planar waveguide device operating in the gigahertz region;[4] alternating layers of AlGaAs and AlAs deposited through chemical vapor provide a stacked dielectric cavity used in distributed feedback lasers.[17] While these methods for creating dielectric structures have found use in commercial products, the potential applications of photonic band gap materials at optical wavelengths have been limited by the difficulty in fabricating three-dimensionally periodic materials with nanometer-scale structures.

Recently, colloidal crystals have received renewed attention as an avenue to achieving controlled dielectric periodicity.[18−21] Colloidal crystals are regular crystalline arrays of highly monodisperse spheres of dielectric materials such as silica or polymers.[22] These materials have been the subject of study for several decades due to their unusual optical[23−28] and thermodynamic

* To whom correspondence should be addressed. E-mail: colvin@rice.edu.

(1) Petrov, E. P.; Bogomolov, V. N.; Kalosha, I. I.; Gaponenko, S. V. *Phys. Rev. Lett.* **1998**, *81*, 77.
(2) Lin, S. Y.; Fleming, J. G.; Hetherington, D. L.; Smith, B. K.; Biswas, R.; Ho, K. M.; Sigalas, M. M.; Zubrzycki, W.; Kurtz, S. R.; Bur, J. *Nature* **1998**, *394*, 251.
(3) Gupta, S.; Tuttle, G.; Sigalas, M.; Ho, K. M. *Appl. Phys. Lett.* **1997**, *71*, 2412.
(4) Lin, S. Y.; Chow, E.; Hietala, V.; Villeneuve, P. R.; Joannopoulos, J. D. *Science* **1998**, *282*, 274.
(5) Holtz, J. H.; Asher, S. A. *Nature* **1997**, *389*, 829.
(6) Lin, V. S. Y.; Motesharei, K.; Dancil, K. P. S.; Sailor, M. J.; Ghadiri, M. R. *Science* **1997**, *278*, 840.
(7) Velev, O. D.; Jede, T. A.; Lobo, R. F.; Lenhoff, A. M. *Nature* **1997**, *389*, 447.
(8) Zakhidov, A. A.; Baughman, R. H.; Iqbal, Z.; Cui, C.; Khayrullin, I.; Dantas, S. O.; Marti, J.; Ralchenko, V. G. *Science* **1998**, *282*, 897.
(9) Holland, B. T.; Blanford, C. F.; Stein, A. *Science* **1998**, *281*, 538.
(10) Davis, S. A.; Burkett, S. L.; Mendelson, N. H.; Mann, S. *Nature* **1997**, *385*, 420.
(11) Imhof, A.; Pine, D. J. *Nature* **1997**, *389*, 948.
(12) Yablonovitch, E. *J. Opt. Soc. Am. B* **1993**, *10*, 283.
(13) Wijnhoven, J. E. G.; Vos, W. L. *Science* **1998**, *281*, 802.
(14) Pan, G.; Kesavamoorthy, R.; Asher, S. A. *J. Am. Chem. Soc.* **1998**, *120*, 6525.
(15) Joannopoulos, J. D.; Meade, R. D.; Winn, J. N. *Photonic Crystals: Molding the Flow of Light*; Princeton University Press: Princeton, NJ, 1995.
(16) Joannopoulos, J. D.; Villeneuve, P. R.; Fan, S. *Nature* **1997**, *386*, 143.
(17) Tanaka, K.; Nakamura, T.; Takamatsu, W.; Yamanishi, M.; Lee, Y.; Ishihara, T. *Phys. Rev. Lett.* **1995**, *74*, 3380.
(18) Asher, S. A.; Holtz, J.; Weissman, J.; Pan, G. *MRS Bull.* **1998**, *October*, 44.
(19) Miguez, H.; Meseguer, F.; Lopez, C.; Blanco, A.; Moya, J. S.; Requena, J.; Mifsud, A.; Fornes, V. *Adv. Mater.* **1998**, *10*, 480.
(20) Bogomolov, V. N.; Prokof'ev, A. V.; Shelykh, A. I. *Phys. Solid State* **1998**, *40*, 594.
(21) Lidorikis, E.; Li., Q.; Soukoulis, C. M. *Phys. Rev. E* **1997**, *55*, 3613.
(22) Pieranski, P. *Contemp. Phys.* **1983**, *24*, 25.
(23) Yoshiyama, T.; Sogami, I. *Phys. Rev. Lett.* **1984**, *53*, 2153.
(24) Sanders, J. V. *Acta Crystallogr.* **1968**, *A24*, 427.
(25) Goodwin, J. W.; Ottewil, R. H.; Parentich, A. *J. Phys. Chem.* **1980**, *84*, 1580.
(26) Krieger, I. M.; O'Neill, F. M. *J. Am. Chem. Soc.* **1968**, *90*, 613.
(27) Hiltner, P. A.; Krieger, I. M. *J. Phys. Chem.* **1969**, *73*, 2386.
(28) Monovoukas, Y.; Gast, A. P. *Langmuir* **1991**, *7*, 460.

10.1021/cm990080+ CCC: $18.00
Published on Web 07/15/1999

properties.[29−35] Colloidal crystals offer a starting point for the fabrication of periodic dielectric materials created through self-assembly rather than lithographic means. Here, one has the potential to create samples with full three-dimensional ordering, a feature important for engineering larger and more complete photonic band gaps. Also, self-assembly methods can create thicker materials than those made using lithography. While the role of sample thickness in the optical properties of colloidal crystals has not been investigated, it is clear that control over this important parameter would be quite valuable in materials engineering. In addition, self-assembly methods are not limited in their length scale, and it is feasible to create materials that are active in the ultraviolet and even the soft X-ray range using colloids with smaller diameters. Finally, as has been demonstrated recently, colloidal crystals provide an ideal scaffold for the creation of both polymeric and inorganic samples with complex porous structures.[7−9,13,36−40] Such samples may exhibit more complete photonic band gaps than silica−air crystals as higher index contrasts are possible; in addition, they also may find applications in catalysis and separation technologies. The success of these nonlithographic routes to the formation of periodic dielectric structures requires the development of robust methods for creating high quality, uniform, and mechanically stable colloidal crystals.

A popular method for creating colloidal crystals is the gravity sedimentation of colloids from dispersions;[19,22,32,41] recent progress in the area has focused on strategies for strengthening the crystals and generating sample formats well suited for optical testing. In one instance, silica colloids were crystallized between parallel plates, and the solvent was then polymerized so as to trap their crystalline order.[42−44] This stabilization comes at a cost, however, as the matrix material has a refractive index closely matched to that of the colloids, thus reducing their diffractive properties. In other work, silica colloids were crystallized in capillaries, and the solvent was allowed to evaporate. The resulting silica−air structures have strong diffractive properties, and transmission spectra can be collected over some regions.[45] Nonetheless, gravity-sedimented samples generally contain polycrystalline domains of unknown sizes.[46,47] In addition, during the gravity sedimentation method, crystal formation can only occur at specific volume fractions of colloids.[22] As a result, array growth is difficult to adjust, and thus film thickness is not easily controlled.

Other methods for ordering colloids into arrays have been explored by investigators seeking to make dense monolayer films of close-packed colloids for nonoptical applications. Under the right conditions, colloid solutions that are spun-coated onto surfaces provide high quality monolayers.[48−52] Convective self-assembly of wetting solutions is also a route for making ordered monolayers and structures of nanocrystals on a variety of substrates.[53] Another method applied to polymer colloids uses the flow of solvent through micromachined channels to create dense colloidal arrays of multiple layers.[37,38,54,55] Finally, recent work by Nagayama et al.[56−65] has exploited capillary forces to drive the assembly of larger ($d > 1\ \mu$m) polystyrene colloids on flat surfaces. This method, which is conceptually similar to the Langmuir−Blodgett methods for film deposition, creates ordered monolayer films on nearly any vertical surface. Under the appropriate solvent and colloid conditions Nagayama et al. showed that patches of bi- and trilayer arrays could also be formed. All of these methods have the advantage of producing well-ordered films on planar surfaces quite rapidly; however, in most instances the deposition techniques have been optimized for the formation of monolayer films.

In this paper a self-assembly technique which relies on capillary forces to organize colloids is used to fabricate colloidal crystal multilayers. These arrays are ordered over long (∼1 cm) length scales and can be fabricated with thicknesses ranging from two layers to several hundred layers. Moreover, the thickness of the resulting sample can be precisely dictated through

(29) Hartl, W.; Klemp, R.; Versmold, H. *Phase Transitions* **1990**, *21*, 229.
(30) Smits, C.; van Duijneveldt, J. S.; Dhont, J. K.; Lekkerkerker, H. N. W. *Phase Transitions* **1990**, *21*, 157.
(31) Aastuen, D. J. W.; Clark, N. A.; Swindal, J. C.; Muzny, C. D. *Phase Transitions* **1990**, *21*, 139.
(32) Davis, K. E.; Russel, W. B.; Glantschnig, W. J. *J. Chem. Soc., Faraday Trans.* **1991**, *87*, 411.
(33) Imhof, A.; van Blaaderen, A.; Maret, G.; Mellema, J.; Dhont, J. K. G. *J. Chem. Phys.* **1994**, *100*, 2170.
(34) Kesavamoorthy, R.; Super, M. S.; Asher, S. A. *J. Appl. Phys.* **1992**, *71*, 1116.
(35) Rundquist, P. A.; Jagannathan, S.; Kesavamoorthy, R.; Brnardic, C.; Xu, S.; Asher, S. A. *J. Chem. Phys.* **1991**, *94*, 711.
(36) Velev, O. D.; Jede, T. A.; Lobo, R. F.; Lenhoff, A. M. *Chem. Mater.* **1998**, *10*, 3597.
(37) Park, S. H.; Xia, Y. *Adv. Mater.* **1998**, *10*, 1045.
(38) Park, S. H.; Xia, Y. *Chem. Mater.* **1998**, *10*, 1745.
(39) Jiang, P.; Hwang, K. S.; Mittleman, D. M.; Bertone, J. F.; Colvin, V. L. *J. Am. Chem. Soc.*, submitted for publication.
(40) Johnson, S. A.; Ollivier, P. J.; Mallouk, T. E. *Science* **1999**, *283*, 963.
(41) Mayoral, R.; Requena, J.; Moya, J. S.; Lopez, C.; Cintas, A.; Miguez, H.; Meseguer, F.; Vazquez, L.; Holgado, M.; Blanco, A. *Adv. Mater.* **1997**, *9*, 257.
(42) Jethmalani, J. M.; Ford, W. T. *Chem. Mater.* **1996**, *8*, 2138.
(43) Jethmalani, J. M.; Sunkara, H. B.; Ford, W. T.; Willoughby, S. L.; Ackerson, B. J. *Langmuir* **1997**, *13*, 2633.
(44) Jethmalani, J. M.; Ford, W. T.; Beaucage, G. *Langmuir* **1997**, *13*, 3338.
(45) Vos, W. L.; Sprik, R.; van Blaaderen, A.; Imhof, A.; Lagendijk, A.; Wegdam, G. H. *Phys. Rev. B* **1996**, *53*, 16231.
(46) Clark, N. A.; Hurd, A. J.; Ackerson, B. J. *Nature* **1979**, *281*, 57.
(47) Okubo, T. *Langmuir* **1994**, *10*, 1695.
(48) Deckman, H. W.; Dunsmuir, J. H. *Appl. Phys. Lett.* **1982**, *41*, 377.
(49) Winzer, M.; Kleiber, M.; Dix, N.; Wiesendanger, R. *Appl. Phys. A* **1996**, *63*, 617.
(50) Burmeister, F.; Schafle, C.; Keilhofer, B.; Bechinger, C.; Boneberg, J.; Leiderer, P. *Adv. Mater.* **1998**, *10*, 495.
(51) Deckman, H. W.; Dunsmuir, J. H. *J. Vac. Sci. Technol. B* **1983**, *1*, 1109.
(52) Hulteen, J. C.; Van Duyne, R. P. *J. Vac. Sci. Technol.* **1995**, *13*, 1553.
(53) O'hara, P. C.; Leff, D. V.; Heath, J. R.; Gelbart, W. M. *Phys. Rev. Lett.* **1995**, *75*, 3466.
(54) Park, S. H.; Qin, D.; Xia, Y. *Adv. Mater.* **1998**, *10*, 1028.
(55) Park, S. H.; Xia, Y. *Langmuir* **1999**, *15*, 266.
(56) Denkov, N. D.; Velev, O. D.; Kralchevsky, P. A.; Ivanov, I. B.; Yoshimura, H.; Nagayama, K. *Nature* **1993**, *361*, 26.
(57) Dimitrov, A. S.; Nagayama, K. *Langmuir* **1996**, *12*, 1303.
(58) Nagayama, K. *Phase Transitions* **1993**, *45*, 185.
(59) Dimitrov, A. S.; Dushkin, C. D.; Yoshimura, H.; Nagayama, K. *Langmuir* **1994**, *10*, 432.
(60) Dushkin, C. D.; Nagayama, K.; Miwa, T.; Kralchevsky, P. A. *Langmuir* **1993**, *9*, 3695.
(61) Adachi, E.; Dimitrov, A. S.; Nagayama, K. *Langmuir* **1995**, *11*, 1057.
(62) Nagayama, K. *Colloids Surf. A* **1996**, *109*, 363.
(63) Dimitrov, A. S.; Nagayama, K. *Chem. Phys. Lett.* **1995**, *243*, 462.
(64) Denkov, N. D.; Velev, O. D.; Kralchevsky, P. A.; Ivanov, I. B.; Yoshimura, H.; Nagayama, K. *Langmuir* **1992**, *8*, 3183.
(65) Yamaki, M.; Higo, J.; Nagayama, K. *Langmuir* **1995**, *11*, 2975.

control of sphere size and concentration in solution. This deposition behavior can be adequately simulated using existing models of film formation developed for monolayer samples. The resulting planar colloidal crystals are highly ordered, and evaporation of the solvent leaves a silica−air array with good optical contrast and mechanical stability. The optical properties of these samples are measured at normal incidence and their qualitative features and trends compared to gravity sedimented colloidal crystals.

Experimental Methods

Materials and Substrates. All solvents and chemicals are of reagent quality and filtered by 0.22 μm syringe filters (Gelman) except for tetraethoxysilane (99%, Alfa) and 3-(trimethoxysilyl)propyl methacrylate (TPM, 98%, Aldrich) which are freshly vacuum distilled before use. The 200 proof ethanol is obtained from Pharmaco Products, and 29.6% ammonium hydroxide is purchased from Fisher. Ultrapure water (18.2 $M\Omega cm^{-1}$) is used directly from a Milli-Q water system. Microslides (75 × 25 × 1 mm, Fisher) are cut into two equal halves along the long sides and are used as substrates. Glass scintillation vials (20 mL, Fisher) are used as experimental cells.

Instrumentation. Scanning electron microscopy is carried out on a software-controlled LEO 440 SEM designed specifically for electron-beam lithography. Transmission spectra are obtained using an Ocean Optics ST2000 fiber optic UV−near-IR spectrometer. A Coulter N4 Plus laser dynamic light scattering (DLS) instrument is used to size the particles. A CrC-100 sputtering system is used to sputter a thin layer (3−4 nm) of gold on samples before SEM analysis.

Colloid Synthesis and Purification. Monodisperse SiO_2 nanospheres are synthesized following the Stober−Fink−Bohn method.[66] Nanospheres with diameters ranging from 200 to 700 nm and relative standard deviations smaller than 7% are obtained through strict control of the reaction conditions.[67] The sizes and size distributions of these samples are obtained from SEM and DLS measurements. Over 200 spheres are sized using SEM in order to arrive at the reported diameters. Before deposition, the silica alcosols are washed with 200 proof ethanol by repeated centrifugation and ultrasonic dispersion cycles in order to remove impurities, such as ammonia, water, and unreacted tetraethoxysilane. Six cycles are usually performed. 3-(trimethoxysilyl)propyl methacrylate (TPM) coated silica is synthesized using a published method[68] and purified as above. All microscopy data presented in this work, however, are from particles without TPM coating. The solvent of deposition, rather than the coating surface, is the key parameter in controlling film deposition.

Experimental Apparatus and Procedures. Prior to use all microslides and scintillation vials are soaked in a chromic−sulfuric acid cleaning solution overnight, rinsed well with ultrapure water from a Milli-Q water system, and dried in a stream of nitrogen. A clean microslide is then placed into 15 mL of purified silica alcosol in a clean scintillation vial. The vial is covered by a 1200 mL crystallizing dish to keep out external airflow and contamination. The entire apparatus is placed on a vibration-free bench in a temperature-controlled laboratory (22 ± 1 °C). For the preparation of these multilayer samples, no substrate withdrawl is necessary. The volume fractions of different samples are determined by drying 6 mL of purified silica alcosol in 80 °C vacuum oven overnight and then weighing the residual solid. 2.04 g/mL is used as the density of silica,[67] though its actual density may be somewhat lower. Then, the samples are diluted or concentrated using a centrifuge−redisperse cycle to the required volume fractions.

For evaluation of the role of sphere size on film formation, six samples (215.2 (3.9%), 298.6 (3.8%), 324.1 (7.2%), 396.6 (5.4%), 437.4 (4.2%), and 508.6 nm (4.3%)) were used. Numbers in parentheses following the sphere diameters refer to the relative standard deviation of the measured diameters. All the samples were placed under the same crystallizing dish to ensure identical ethanol evaporation rates. Samples with volume fractions of 0.1%, 0.5%, 1.0%, 1.5%, 2.0%, and 3.0% and the same particle size (298.6 nm (3.8%)) were used to determine the effect of volume fraction on the film thickness. Samples (215.2 (3.9%) and 279.2 nm (4.6%)) with volume fractions of 1% were used to determine the effect of solvent evaporation rate on the film thickness. Duplicates of each sample were tested under three different evaporation conditions: open to ambient atmosphere, covered in a crystallizing dish, and covered in a crystallizing dish with a small amount of ethanol (20 mL in a 50 mL beaker). One of the duplicates was used to determine the evaporation rate by weighing the vial on a digital analytical balance. The typical solvent evaporation rate, given in units of volume per time, was found to be 9×10^{-4} cm^3/min.

Thicker films are fabricated by successive dip coatings. After each single coating is deposited, the film is air-dried for at least 24 h and dipped again into another purified silica alcosol with the same particle size. The coating and drying cycle can be repeated to systematically increase film thickness.

Characterization of Colloidal Crystal Films. Scanning electron microscopy (SEM) is used to determine the film thickness. A thin layer of gold is sputtered onto the samples prior to imaging. To reveal an edge appropriate for cross-sectional analysis, samples are scraped using a sharp razor blade. By tilting the specimen 30−40°, it is possible to image this edge and quantify film thickness; 10 random locations from the center square centimeter of the sample are analyzed for thickness. Optical properties of the silica colloidal single-crystal films are evaluated by measuring their transmission spectra at normal incidence, using an Ocean Optics ST2000 fiber optic UV−near-IR spectrometer.

Results

Crystalline quality is among the most important parameters in determining the performance of colloidal crystals in optical applications. The formation of point defects or domains can have an enormous impact on the diffraction properties. Figure 1A shows a typical SEM image of a single crystal of colloidal silica with a 298.6 nm diameter, grown using the methods described above. This sample exhibits an ordered close-packed arrangement of silica colloids over a sample area of 10 μm which extends over an even larger area; this can be illustrated by the two-dimensional Fourier transform of a low-magnification SEM image. Such data is shown in the inset of Figure 1A. The sharp peaks confirm the presence of long-range crystalline order, extending over the largest length scales (40×40 μm^2) accessible in a single low-magnification image. Perfectly ordered films can be made for a variety of sphere diameters. Parts A and B of Figure 4 show SEM images of two crystals with different particle sizes (206.4 and 437.4 nm, respectively). As in Figure 1A, long-range order is confirmed by Fourier transform of low magnification images (insets to Figure 4).

It is a challenge to use microscopy for proof of sample order over centimeter distances. Lower magnification images do not have the spatial resolution needed to identify distinct colloids; one approach is to compare micrographs of 40 μm^2 areas collected as a sequence during the translation of the sample. If domain boundaries are observed during this movement, then the

(66) Stober, W.; Fink, A.; Bohn, E. *J. Colloid Interface Sci.* **1968**, *26*, 62.
(67) Bogush, G. H.; Tracy, M. A.; Zukoski IV, C. F. *J. Non-Cryst. Solids* **1988**, *104*, 95.
(68) Philipse, A. P.; Vrij, A. *J. Colloid Interface Sci.* **1989**, *128*, 121.

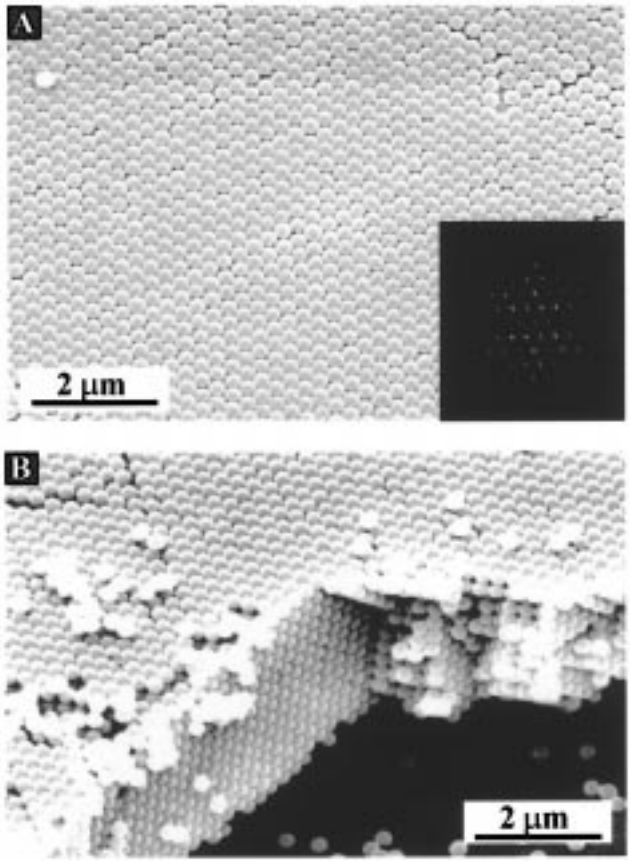

Figure 1. (A) Typical scanning electron micrograph (SEM) of a sample (top view) showing spheres of 298.6 nm diameter. The inset shows a Fourier transform of a 40 × 40 μm^2 region. (B) Typical SEM side view of the same sample at the same magnification (×12 000), showing a perspective view of the cleaved face and the underlying substrate.

hexagonal registry of the images evident in their FFTs will not be aligned. Figure 2 shows such data for four representative images taken at the edges of a 4 mm square. The alignment of the spots in all four images illustrates the registry of the array lattice over these long length scales. Morevoer, analysis of many intermediate images also showed perfect alignment and no evidence of any grain boundaries.

While order within the plane parallel to the glass substrate is important for the optical properties of the films, especially when they are evaluated away from normal incidence, the stacking of close-packed layers perpendicular to the substrate is responsible for the diffraction observed in normal-incidence transmission measurements. To evaluate this issue, colloid films can be abraded to reveal their stacking perpendicular to the substrate as shown in Figure 1B. This cross-section shows that the close-packed structure extends uniformly over the 15 layers shown; Figure 8B shows a thicker 50 layer sample which also exhibits a regular arrangement from the top surface to the bottom surface. The visual appearance of the samples (see Figure 3) is a testament to this high crystalline quality and the uniform thickness of these films.

To form high quality planar crystals, particle size distribution (S.D.) is a crucial factor. This is illustrated in Figure 5, which shows SEM images of two samples with different size distributions (3.8% and 14.2% relative standard deviations, respectively). The sample with

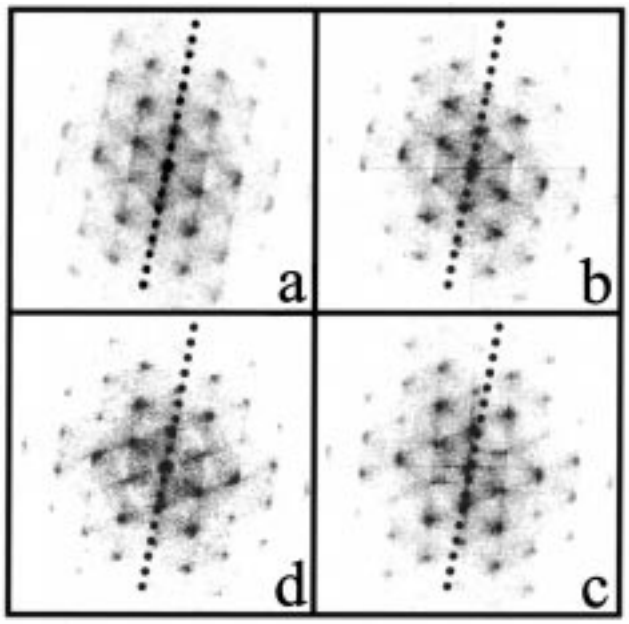

Figure 2. Fourier transforms (FFT) of four 11.75 × 11.75 μm^2 regions of a 1 cm^2 colloidal silica single crystal. These images were part of a series taken every 50 μm over a 4 × 4 mm square region; they represent the four corners and image c was closest to the edge of the sample. The four parallel dashed lines indicate one reference direction, and demonstrate that the four images are roughly of the same orientation, as were all intermediate images. Within a 4 × 4 mm^2 region, the largest deviation from this orientation is ~1.6 degrees, represented in image c. This demonstrates that the crystallographic orientation of the sample is preserved over this entire region.

a narrow size distribution exhibits order over a long length scale and sharp peaks in the Fourier transform of a low-magnification SEM image; the polydisperse sample has only short-range order and exhibits rings in the Fourier transform. Films that lack crystalline quality, such as the one shown in Figure 5B, even when relatively thin, are white and opaque. This is in sharp contrast to the brilliant color and transparency apparent in more ordered films (Figure 3). Data collected from over 20 samples suggest that when this method is used, colloids must have a size distribution with relative standard deviation less than 8% (on the diameter) in order to form high quality close-packed crystals and thus good optical samples.

For this deposition process, two parameters allow for control of film thickness (or number of colloidal layers): particle diameter (d) and particle volume fraction (V.F.). Figure 6 shows how film thickness varies with these two parameters. For these measurements layer thickness is determined using cross-sectional SEM images of the types shown in Figures 1B, 7, and 8. Particle size affects the film thickness in a systematic way: for the same volume fraction, a solution of larger particles yields fewer layers. Two examples are shown in Figure 7, and the relationship is quantified in Figure 6A. Particle volume fraction also affects film thickness (Figure 6B); more concentrated colloidal solutions leave thicker multilayer deposits (Figure 8). Because film uniformity degrades significantly when colloidal solutions of more than 4% volume fraction are used, the formation of thicker films requires multiple coating. In this approach, samples are allowed to dry and then are

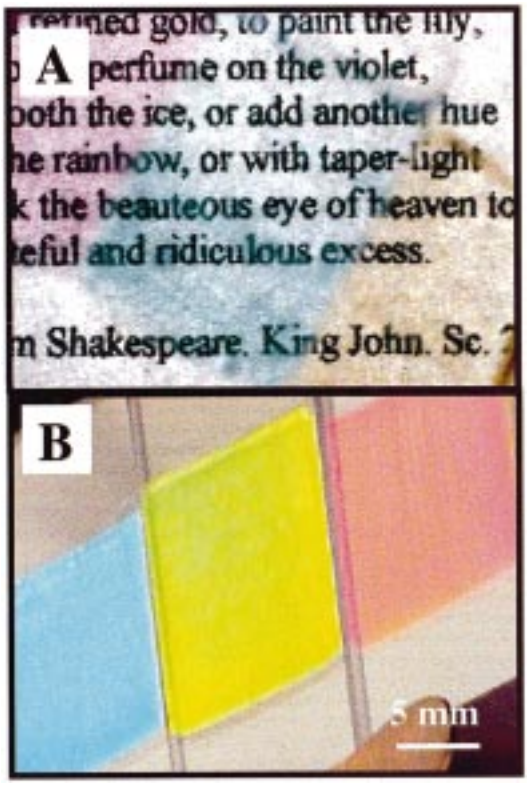

Figure 3. (A) Photograph of three samples with different sphere diameters (307.2, 353.0, and 383.7 nm, from left to right). The samples are clear and highly uniform. (B) Photograph of the same samples illuminated with white light.

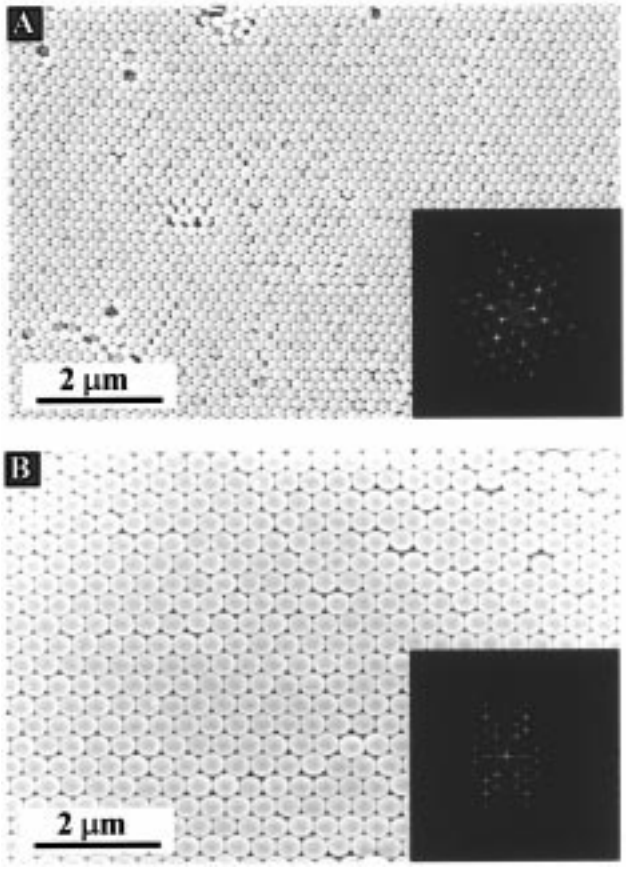

Figure 4. SEM images of two samples with different particle diameters (×12 000 magnification). The insets show Fourier transforms of 40 × 40 μm^2 regions. Key: (A) d = 206.4 nm; (B) d = 437.4 nm.

reimmersed in the colloidal solutions; new colloidal multilayers form easily on top of the original ones and the process can be repeated many times with the thickness increasing linearly after each deposition. Figure 9 shows a scanning electron micrograph of a portion of a multicoated sample.

The optical properties of these films can be evaluated using visible−near-IR transmission in normal incidence. Figure 10 shows scaled absorption spectra vs particle size for a wide range of colloidal sphere diameters. Two notable features of the spectra are sharp peaks due to the Bragg diffraction of visible light from the ordered spheres and a background rising at shorter wavelengths. The systematic change in color seen in transmission and reflection of uniform films of different particle sizes (see Figure 3) is due to Bragg diffraction. Figure 11 shows the changes in the optical transmission spectra of films of different thickness made using equal sized particles. The background has been subtracted in these data so that they can be compared easily. The intensity of the diffracted peak increases approximately linearly with the number of layers, although this is not evident in Figure 11 because the data have been scaled to uniform height. Also, the peak widths narrow as sample thickness is increased. Finally, Fabry−Perot fringes (indicated by the arrows in Figure 11) become smaller and more closely spaced in thicker samples.

Discussion

Crystal Structure of Planar Arrays. SEM images of the top view of these samples show that the colloids are arranged in a close-packed fashion, with each sphere touching six others in one layer (Figures 1 and 4). This close-packing arrangement is well-known in crystals comprised of colloids, such as these silica spheres, whose ionic interactions are minimal.[69,70] In this close-packed geometry, whether the structure is face-centered cubic (ABCABC...), hexagonal close-packed (ABABAB...), or randomly stacked, these images illustrate that the samples are oriented with their (111) axes parallel to the substrate.

Exact characterization of the crystal structure of these samples from SEM micrographs alone is problematic. Though images such as these confirm a regular close-packed arrangement (Figures 1B, 7, and 8), they cannot be used to distinguish between the fcc and hcp structures. This is because it is difficult to determine the exact angle of the cross-sectional view, which in turn makes it difficult to assess which crystal face is visualized in these images. Confocal microscopy of gravity sedimented colloidal crystals[71] has indicated that the stacking between (111) planes is neither fcc nor hcp but is instead a random arrangement. Theoretical calculations, though, have indicated that the fcc structure is stabilized slightly even with completely noninteracting spheres.[72,73] In future studies, where the transmission

(69) Tsunekawa, S.; Barnakov, Y. A.; Poborchii, V. V.; Smoilovich, S. M.; Kasuya, A.; Nishina, Y. *Microporous Mater.* **1996**, *8*, 275.
(70) Miguez, H.; Meseguer, F.; Lopez, C.; Mifsud, A.; Moya, J. S.; Vazquez, L. *Langmuir* **1997**, *13*, 6009.
(71) van Blaaderen, A.; Ruel, R.; Wiltzius, P. *Nature* **1997**, *385*, 321.
(72) Woodcock, L. V. *Nature* **1997**, *385*, 141.

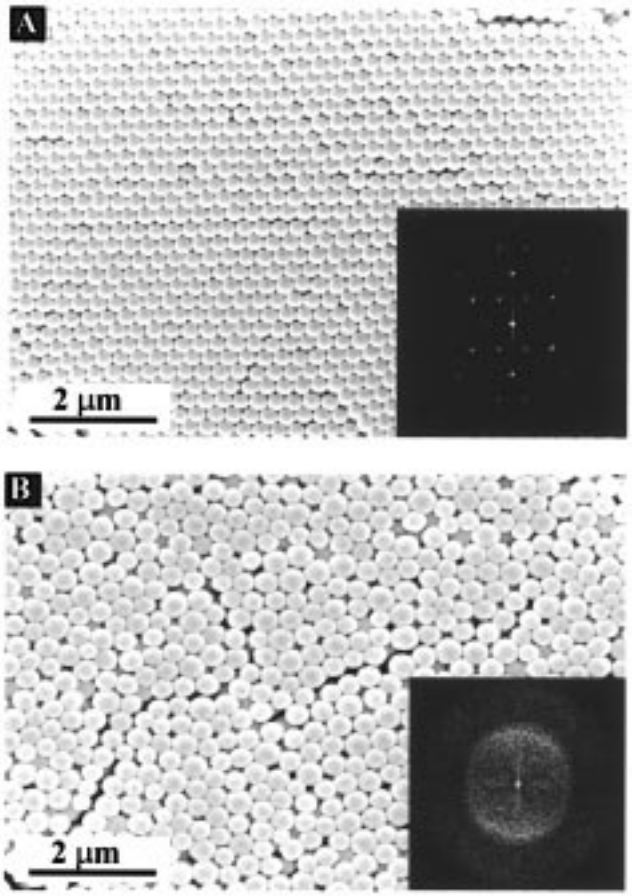

Figure 5. SEM images of two samples with different particle size distributions (S.D.) (×12 000 magnification). The insets show Fourier transforms of 40 × 40 μm^2 regions. (A) S.D. = 3.8%; (B) S.D. = 14.2%.

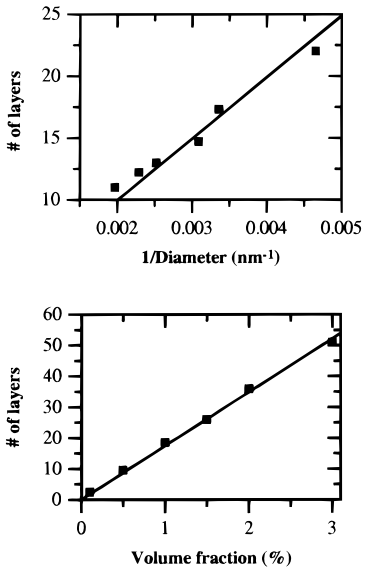

Figure 6. (A, top) Number of layers vs the inverse of the particle diameter, for samples grown from a 1% V.F. solution. (B, bottom) Number of layers vs the particle volume fraction, d = 298.6 nm.

is investigated as a function of angle away from the normal, the exact nature of the crystal structure will be a more important issue.[26,27]

(73) Bruce, A. D.; Wilding, N. B.; Ackland, G. J. *Phys. Rev. Lett.* **1997**, *79*, 3002.

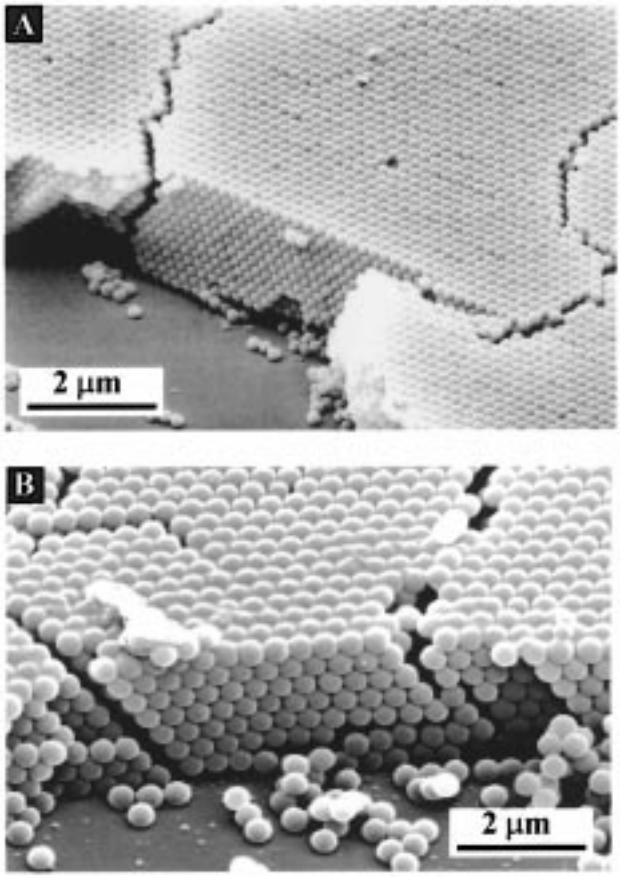

Figure 7. SEM cross-sectional images of two samples with different particle diameters, grown from solutions with the same volume fraction (0.5%). The 206.4 nm particle size produced a film with 14 layers (A), and a 396.6 nm particle size produced a film with 7 layers (B).

Domain Size of Planar Arrays. An important feature of these samples is their long-range order within the plane parallel to the substrate. In gravity-sedimented colloidal crystals, there can be some preferential alignment of the crystal axes with the capillary sidewalls; however, such samples are multicolored under white light illumination[74] and are thought to contain colloidal crystal domains whose (111) axes are not aligned. In contrast, the multilayer samples described here are deposited onto a flat substrate which forces their (111) axes to be aligned over distances of millimeters (Figure 2). For this reason, when viewed at a variety of angles, the color of the entire film is uniform (Figure 3). Thus, unlike the gravity-sedimented colloidal crystals which are polycrystalline in most instances,[46,47] these samples consist of a single crystalline close-packed array.[75] We note that in this work when samples with slightly broader size distributions (>8%) are deposited, grain boundaries in the plane parallel to the substrate are observed; similarly, Nagayama et al. observed grain boundaries in monolayers of colloids with 10−15% distributions in size.[57] This suggests that the monodispersity of the colloids, rather than the deposition process itself, is responsible for their long-range ordering.

Perfection of Colloidal Crystals. Though these samples are single crystals, they are not perfect crystals

(74) Gast, A. P.; Russel, W. B. *Phys. Today* **1998**, *51* (12), 24.
(75) Parker, S. P. *Dictionary of Scientific and Technical Terms*, 4th ed.; McGraw-Hill Book Company: New York, 1989.

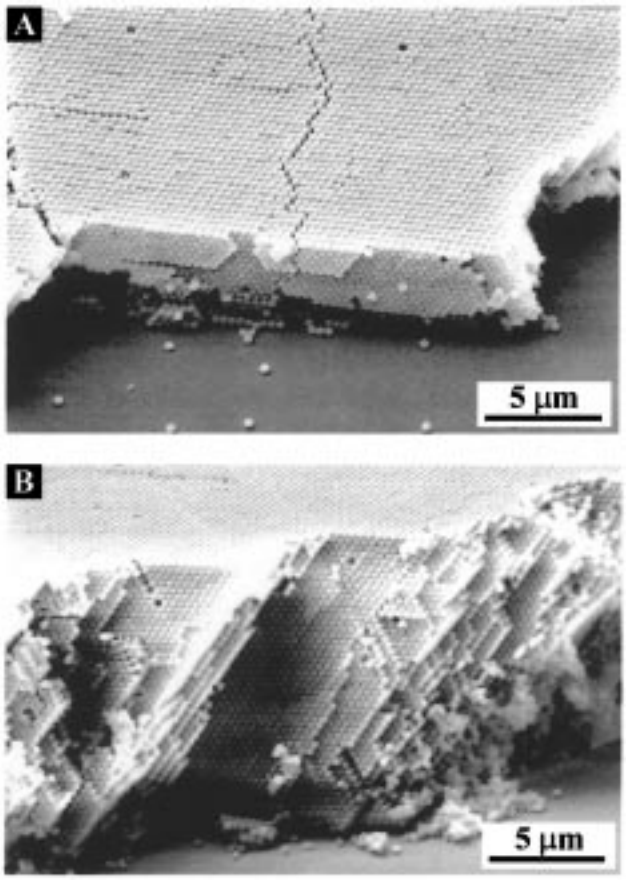

Figure 8. SEM cross-sectional images of two samples grown from solutions with different particle volume fractions. In both parts A and B, the spheres are 298.6 nm in diameter. (A) V.F. = 0.8%, 18 layers; (B) V.F. = 3.0%, ~50 layers.

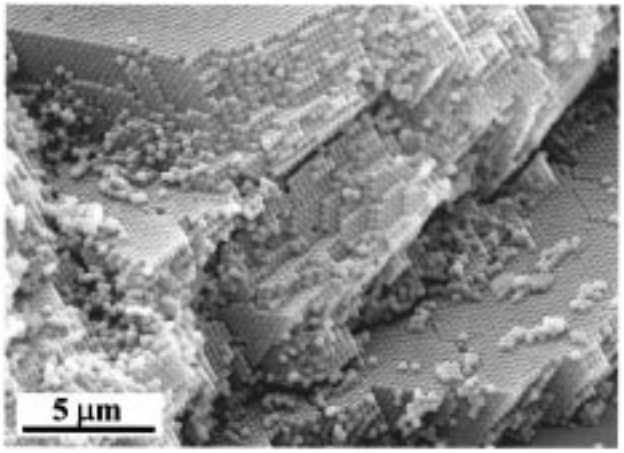

Figure 9. Typical SEM image of a sample (d = 279.2 nm) deposited with four successive coatings. Each deposition provides 12 colloidal monolayers.

as is clear from the SEM photographs. Two types of defects are observed routinely in the SEM images of these samples. The first is sphere vacancies that appear every ~10 μm on average. The second is vertical cracks in the crystal, perpendicular to the glass substrate. Examples may be seen in Figures 7A and 8A. Cracks are typically observed every 10 μm in most samples and unlike a classic grain boundary, the registry of the hexagonal packing is preserved across these features. One explanation for the cracking is that the deposition of metal and the subsequent exposure of films to the

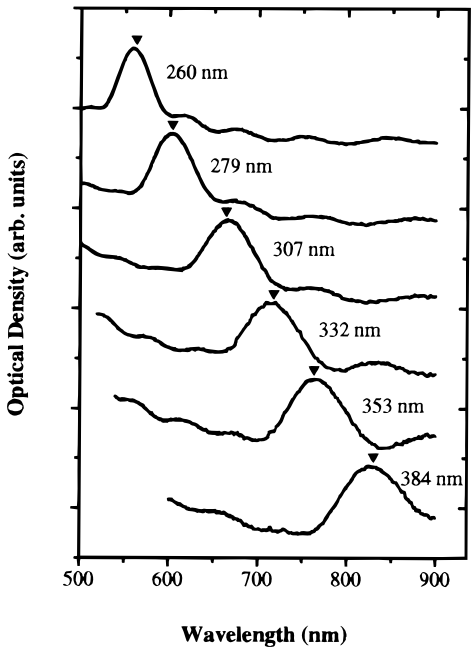

Figure 10. Normal incidence transmission spectra (optical density) of samples with different sphere diameters, determined using SEM analysis. These curves have been scaled to a constant height, and vertically offset for clarity. The arrows indicate the expected positions of the peaks for each curve, calculated using Bragg's law at normal incidence and the diameters shown. Typically at the peak maximum only 10−20% of the incident light is transmitted.

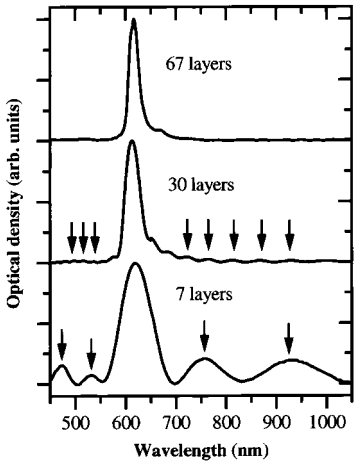

Figure 11. Normal incidence transmission spectra (optical density) of three samples (d = 279.2 nm) with increasing film thickness. These curves have been scaled to a constant height, and vertically offset for clarity. Thicker samples exhibit more closely spaced (and smaller) Fabry−Perot fringes. The arrows indicate local maxima, λ_p, chosen for thickness analysis, with the longest wavelength as $p = 0$ (see supplemental Figures 1 and 2). In addition, a rising background apparent in the data of Figure 10 has been subtracted from these data; for samples of more than 20 layers, this background contributes at most 20% of the rejection of light at the peak maximum.

high vacuum of the SEM damages their structure and induces cracking; to evaluate this issue, atomic force microscopy (AFM) of the same materials was performed under ambient conditions on the as-prepared surfaces. Though cracks were still observed, they were fewer in number and typically found every 100 μm. The drying tension in thin colloidal films is well-known to cause

cracking of much thinner deposits;[76] it is likely that such drying-induced shrinkage is responsible for this problem as well. Strategies for minimizing this effect include the addition of surfactants, and better control over the drying conditions.

Controlling Film Thickness. One of the great advantages of this method of colloidal crystal formation is its ability to create samples with precisely controlled thickness. By controlling such parameters as colloidal concentration and sphere size, it is possible to vary the thickness of the films from a few layers to hundreds of layers. The representative images in Figures 7 and 8 suggest that film thickness, T, is related to the deposition parameters in a systematic way. Figure 6 illustrates the quantitative relationships between the number of colloidal layers, k, and the deposition parameters φ (volume fraction of colloids in solution) and d (colloid diameter).

These trends can be understood using a model developed by Nagayama et al.[56−65] for the self-assembly of *monolayer* colloidal films. In his experiments, which are reminiscent of Langmuir−Blodgett methods for self-assembly, a vertical or slanted substrate is withdrawn from a solution of polystyrene colloids at a constant rate. A meniscus region is formed on the substrate due to wetting by the solution; evaporation of the solvent out of this thin meniscus leads to a constant solution influx, which draws colloids into the area of film formation. During the solvent evaporation these colloids experience interparticle capillary forces which organize them into close-packed arrays. The resulting thickness is then entirely dependent on the flux of particles into the meniscus, and mass balance can be used to derive a simple formula for array thickness.

The film formation conditions used by Nagayama et al. were optimized for the production of uniform colloidal monolayers; however, it is possible to adapt this formalism to the formation of multilayer films. To create thick films, the array growth rate, which is a balance of the solvent evaporation and substrate withdrawal rates, must be as small as possible. Thus, the slowest possible array growth results when the substrate is not mechanically withdrawn. Under this circumstance the array growth rate and the solvent evaporation rate are equal. This leads to a prediction that the final multilayer thickness depends on the deposition parameters according to[77]

$$k = \frac{\beta \mathbf{L} \varphi}{0.605 d(1 - \varphi)} \qquad (1)$$

where k is the number of layers, **L** is the meniscus height, β is the ratio between the velocity of a particle in solution and the fluid velocity and is taken to be 1, d is the particle diameter, and φ is the particle volume fraction in solution. The data shown in Figure 6 clearly demonstrate that the basic trends predicted by this equation are valid. A surprising result from the model is that the final array thickness is not dependent on the solvent evaporation rate. This is because, while faster solvent evaporation does lead to faster array formation, it also leads to increased solution influx into the array growth region. This increased influx of silica colloids balances the faster growth rate, leading to a film thickness independent of evaporation rate. This prediction was verified experimentally by creating multilayer samples under different evaporation conditions. While film uniformity was somewhat dependent on evaporation rate, film thickness was not. In addition, film thickness was insensitive to the surface derivatization of the colloids.

An important issue in this method is the role that the solvent plays in controlling the deposition of colloidal multilayers. The solvent enters into the model through the parameter **L** that is defined as the height of the meniscus over which evaporation occurs. In the case of the ethanolic solutions used in this work, this parameter can be extracted from linear fits to the data shown in Figure 6. Assuming a β of 1, the data in Figure 6A provides an **L** value of 316 μm while the data in Figure 6B gives an **L** value of 301 μm. Similar evaporation lengths, on the order of 200 μm, were reported for the growth of polystyrene colloidal monolayers from water.[63] While this parameter cannot be exactly computed, an upper limit for its value can be found by considering the meniscus height of ethanol on a flat glass surface. Using the surface tension of ethanol and its contact angle for wetting glass, it is possible to calculate a meniscus height of 3500 μm.[78] As expected, the observed meniscus height of ~310 μm is smaller than the value for a flat substrate as the film must wet a rough surface of colloids. This analysis suggests that solvents such as water, which have large surface tensions and even lower contact angles, should deposit thicker films than the corresponding ethanolic solutions. Attempts to deposit silica colloids from aqueous solutions did lead to thicker films, but these samples had poor uniformity.

Measuring Multilayer Thickness Using Optical Techniques. Multilayer thickness is an important parameter for quantitative assessment of sample optical properties. While scanning electron microscopy (SEM) provides a measure of this parameter, it is a destructive method as it requires the deposition of a thin gold coating on the sample. A less time-consuming and nondestructive method is an optical technique which uses the Fabry−Perot (FP) fringe[79] positions to analyze for film thickness. These fringes result from interference between reflections from the top and bottom surfaces of the sample and are indicated by the arrows in Figure 11. An analysis, using Bragg's law, of the spectral positions of these local maxima permits an accurate determination of sample thickness (Supporting Figure 1). The thickness determined from this optical technique is in excellent agreement with thickness found from cross-sectional SEM (Supporting Figure 2).

Thickness Uniformity in Multilayer Samples. An important feature of this deposition method is that it allows for the systematic control over multilayer thickness (Figure 6). Indeed, the preparation of such well-

(76) Bergna, H. E. *The Colloid Chemistry of Silica*; Bergna, H. E., Ed.; American Chemical Society: Washington, DC, 1994; Vol. 234, p 376.

(77) This equation was derived from eq 7 from Nagayama et al.[57] by allowing the evaporation rate, j_e, to be equal to the array growth rate, v_c.

(78) Hiemenz, P. C. *Principles of Colloid and Surface Chemistry*; Marcel Dekker: New York, 1984; p 278.

(79) Hecht, E. *Optics*, 2nd ed.; Addison-Wesley Publishing Company: Reading, MA, 1987.

controlled materials now makes it possible to evaluate many thickness-dependent properties of these systems. For this work to proceed, however, it is important to assess the uniformity of the film thickness over the entire area of the sample. One way to characterize the thickness distribution is to rely on the statistical analysis of cross-sectional SEM images. Films are typically abraded along a diagonal, and it is possible to collect cross-sectional data at many points over the entire central region (~5 mm) of the sample. The standard deviation found for thickness in these measurements is on the order of 10%. A complementary method for analyzing film thickness uniformity is to rely on the optical techniques to assess film thickness (Supporting Figures 1 and 2). Simulations of the interference effect indicate that if the thickness of the sample in the optical path varies by more than ±10%, then well-defined maxima and minima will not be observed. Thus, the observation of well-defined fringes (Figure 11) demonstrates that film thickness deviates less than 10% on average.

The Optical Properties of Colloidal Crystal Multilayers. The basic features of the normal incidence optical spectrum of these colloidal crystal multilayers are in good agreement with those observed for gravity-sedimented samples. Figure 10 shows how the peak in the optical spectum depends on sphere diameter. When the wavelength of incident light satisfies the Bragg condition, it is diffracted away from the propagation axis, leading to a decrease in the transmission and thus a peak in the absorption spectrum. The position of this peak can be related to the sphere diameter and the effective refractive index of the medium using $\lambda_{max} = 2n_{eff}d_{111}$, where d_{111} is the interlayer spacing.[80] The arrows that are shown in Figure 10 are peak positions predicted from this equation using sphere sizes as determined from SEM; agreement with experimental data is quite good.

While this simple diffraction theory can predict the peak positions, it is unable to provide a quantitative explanation for any of the other features in the spectra. Recently, several groups have attempted to adapt the dynamical theory of X-ray diffraction to this purpose.[42,43,45,81−83] However, this theory is based on the approximation that the refractive index contrast between the scattering centers and the interstitial medium is quite small, on the order of 10^{-4}, an approximation not valid for these silica−air crystals. For this reason, a detailed analysis of the shapes and intensities of the optical transmission function must rely on more complete treatments of scattering from periodic dielectrics. Theories of the optical properties of photonic band gap materials provide an avenue for this understanding; this issue has been explored more fully elsewhere.[84]

An important feature of these spectra is the rising background that grows at shorter wavelengths; this causes the samples to look slightly hazy and could place limits on their use in many optical applications. This background has been observed, but rarely discussed, in gravity-sedimented crystals as well, and its origins remain obscure. While it does not clearly fit the λ^{-4} dependence expected for Rayleigh scattering, defects or sphere surface roughness could give rise to this phenomenon. Alternatively, it may represent the collective effect of diffraction off of all of the lattice planes other than the (111) planes.[85] If so, it is an intrinsic property of any periodic array of spheres, not merely of self-assembled colloidal crystals.

An interesting feature of the optical spectra is the increase in peak width as sample thickness is decreased (Figure 11). This effect is similar to the Debye−Scherrer broadening of X-ray diffraction peaks in small crystallites;[86] however, the widths reach a limiting value of only ~40 nm in thick samples. A full treatment of the thickness-dependent optical effects of these samples is the subject of a forthcoming publication.[87]

Conclusion

Using a simple method, it is possible to deposit planar single crystals of nanosphere arrays on a wide variety of substrates. Scanning electron microscopy (SEM) of the samples shows a close-packed structure and single-crystal quality throughout the film. The number of nanospheres deposited can be widely varied with this method; film thicknesses ranging from single monolayers to 100 layers are easily created through control over the particle volume fraction and sphere size. The planar format and uniformity of these materials make them ideally suited for optical characterization. The qualitative features of their spectra are in good agreement with simple models of diffraction.

Acknowledgment. The authors would like to acknowledge funding from the NSF (CHE-9702520) and the Welch Foundation (C-1342). V.L.C. would like to thank D. M. Mittleman for many useful discussions concerning the optical properties of these materials.

Supporting Information Available: Figures showing an analysis, using Bragg's law, of sample thickness (Supporting Figure 1) and correlation of SEM with Bragg's Law thickness (Supporting Figure 2). This material is available free of charge via the Internet at http://pubs.acs.org.

CM990080+

(80) For close-packed spheres, the interlayer spacing is related to the sphere diameter, ***D***, by $d_{111} = (2/3)^{1/2}D$.

(81) Monovoukas, Y.; Fuller, G. G.; Gast, A. P. *J. Chem. Phys.* **1990**, *93*, 8294.
(82) Rundquist, P. A.; Photinos, P.; Jagannathan, S.; Asher, S. A. *J. Chem. Phys.* **1989**, *91*, 4932.
(83) Sunkara, H. B.; Jethmalani, J. M.; Ford, W. T. *Hybrid Organic−Inorganic Composites*; Mark, J. E., Lee, C. Y.-C., Bianconi, P. A., Ed.; American Chemical Society: Washington, DC, 1995; Vol. 585, p 181.
(84) Mittleman, D. M.; Bertone, J. F.; Jiang, P.; Hwang, K. S.; Colvin, V. L. *J. Chem. Phys.* **1999**, *111*, 345.
(85) Liu, L.; Li, P.; Asher, S. A. *J. Am. Chem. Soc.* **1997**, *119*, 2729.
(86) Cullity, B. D. *Elements of X-ray Diffraction*, 2nd ed.; Addison-Wesley Publishing Company, Inc.: Reading, MA, 1978.
(87) Bertone, J. F.; Jiang, P.; Hwang, K. S.; Mittleman, D. M.; Colvin, V. L. *Phys. Rev. Lett.*, in press.